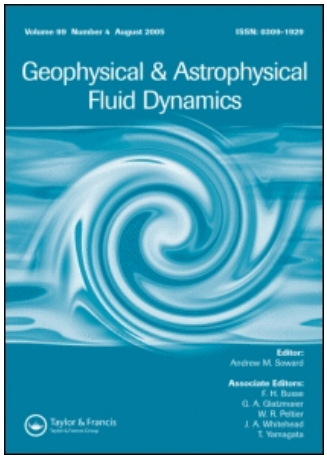

Geophysical & Astrophysical Fluid Dynamics
Publication details, including instructions for authors and subscription information:
http://www.informaworld.com/smpp/title~content=t713642804

On the adjustment to the Bondi-Gold theorem in a spherical-shell fast dynamo

R. Hollerbach [a]; D. J. Galloway [b]; M. R. E. Proctor [c]
[a] Department of Mathematics, University of Glasgow, Glasgow, UK
[b] School of Mathematics and Statistics, University of Sydney, Sydney, Australia
[c] Department of Applied Mathematics and Theoretical Physics, University of Cambridge, Cambridge, UK

Online Publication Date: 01 March 1998
To cite this Article: Hollerbach, R., Galloway, D. J. and Proctor, M. R. E. (1998) 'On the adjustment to the Bondi-Gold theorem in a spherical-shell fast dynamo', Geophysical & Astrophysical Fluid Dynamics, 87:1, 111 - 132
To link to this article: DOI: 10.1080/03091929808208996
URL: http://dx.doi.org/10.1080/03091929808208996

Geophys. Astrophys. Fluid Dynamics, Vol. 87, pp. 111–132
Reprints available directly from the publisher
Photocopying permitted by license only

ON THE ADJUSTMENT TO THE BONDI-GOLD THEOREM IN A SPHERICAL-SHELL FAST DYNAMO

R. HOLLERBACH[a], D. J. GALLOWAY[b] and M. R. E. PROCTOR[c]

[a]*Department of Mathematics, University of Glasgow, Glasgow, G12 8QW UK;* [b]*School of Mathematics and Statistics, University of Sydney, Sydney, NSW 2006 Australia;* [c]*Department of Applied Mathematics and Theoretical Physics, University of Cambridge, Cambridge, CB3 9EW UK*

(Received 10 March 1997; In final form 2 May 1997)

We present a numerical solution of the magnetic induction equation in a spherical fluid shell, with an insulator inside and outside. Prescribing an axisymmetric, time-dependent, chaotic flow, we find that the magnetic field appears to grow on the fast advective, rather than on the slow diffusive time scale. We demonstrate how this may be reconciled with the theorem of Bondi and Gold (1950), that the potential field in these insulators inside and outside the shell cannot be amplified on the fast time scale, by having the field become increasingly contained within the shell with increasing magnetic Reynolds number. Thus, as the Bondi-Gold theorem becomes more and more applicable, there is indeed less and less external field being amplified. This is in precise agreement with the conjecture of Rädler (1982) that the resolution would be to have an "invisible dynamo," one having no external field. Finally, we consider some of the implications of this adjustment for the different symmetries of the field (dipolar versus quadrupolar) and the flow ($\mathbf{u}$ versus $-\mathbf{u}$).

Keywords: Kinematic fast dynamos; Bondi-Gold theorem

1. INTRODUCTION

In view of the ubiquity of magnetic fields in astrophysics (Parker, 1979), it is of interest to consider the mechanism by which these fields are created. It is generally recognized that they are created by the dynamo action of fluid motions in the electrically conducting plasma.

The equation governing this dynamo action is the magnetic induction equation,

$$\frac{\partial}{\partial t}\mathbf{B} = \nabla \times (\mathbf{u} \times \mathbf{B}) + R_m^{-1}\nabla^2\mathbf{B}, \tag{1.1}$$

here nondimensionalized such that the advective time scale is O(1) and the diffusive time scale is $O(R_m)$. In astrophysical situations this magnetic Reynolds number R_m is typically very large, perhaps $10^8 - 10^{10}$. There is thus quite a disparity of time scales in the induction equation, and this disparity leads to some very interesting physics, aspects of which we will consider in this work.

For example, will the fluid flow **u** amplify the field **B** on the fast advective, on the slow diffusive, or perhaps on some intermediate time scale? It is precisely this question that lead Vainshtein and Zeldovich (1972) to introduce the concept of fast versus slow dynamos. A flow **u** is said to be a fast dynamo if it amplifies the field on the fast time scale; if it amplifies the field on some slower time scale it is only a slow dynamo. More formally, consider how the growth rate of **B** behaves in the limit as the magnetic Reynolds number tends to infinity: the flow is a fast dynamo only if this growth rate tends to some nonzero value. Now, it turns out that astrophysical magnetic fields are often observed to evolve on the fast time scale, and it is this that motivates the interest in fast dynamos. See for example Childress and Gilbert (1995) for a general discussion of fast dynamo theory.

In this work we consider fast dynamo action in spherical geometry. We present a numerical code designed to solve the induction equation in a spherical shell, for a particular class of kinematically prescribed flows **u**. Previous numerical studies of this kind include work in three-dimensional flows in planar geometry (Galloway and Frisch, 1986) and in spherical geometry (Dudley and James, 1989; Zheligovsky, 1993), and in two-dimensional flows in planar geometry (Galloway and Proctor, 1992; Otani, 1993; Ponty *et al.*, 1995) and in spherical geometry (Hollerbach *et al.*, 1995). In this work we present in greater detail the model of Hollerbach *et al.* (1995), hereafter referred to as paper I. We will show that as we increase R_m up to 10^5 for several different flows, the growth rates of the eigensolutions we obtain do

seem to tend to nonzero values, indicating that these flows are acting as fast dynamos.

The particular interest in considering fast dynamo action in a bounded domain such as a spherical shell is due to a theorem of Bondi and Gold (1950), stating that the (unsigned) flux through the boundaries of one's domain, and hence the potential field outside them, cannot grow on the fast time scale. To derive the Bondi-Gold theorem, we begin by recalling the frozen flux theorem, which states that in the limit $R_m \equiv \infty$ a flow will advect magnetic field lines as material lines, frozen into the fluid. [See for example Moffatt (1978) for a proof of this result.] An immediate consequence of frozen flux is then that the unsigned flux through any material surface remains constant. Applied to the particular material surfaces that constitute the boundaries of one's domain*, one obtains the above result. Formally, the Bondi-Gold theorem thus states that in the limit $R_m \equiv \infty$ the so-called pole strength $\int |\mathbf{B} \cdot \hat{\mathbf{n}}| \, dS$ remains constant in time. The purpose of this work is to consider how the adjustment to the Bondi-Gold theorem occurs in the limit $R_m \to \infty$.

That the Bondi-Gold theorem poses a potential problem for bounded fast dynamos has been noted previously by Moffatt (1979) and by Rädler (1982), and is evident when one notes that at any finite magnetic Reynolds number the induction equation will always settle down to a well-defined eigensolution, in which all parts grow at the same rate. In particular, whatever external potential field there may be will necessarily grow at the same rate as the internal field. Having just demonstrated that the external field cannot grow on the fast time scale, one might conclude that the internal field also cannot grow on the fast time scale, that is, that bounded fast dynamos do not exist.

However, Rädler (1982) then conjectured further that bounded fast dynamos might nevertheless exist, provided they adjust themselves so that they simply have no external field, the so-called "invisible dynamo." If the eigensolutions adjust themselves so that their external fields tend to zero as the magnetic Reynolds number tends to infinity, the Bondi-Gold theorem will be met, even though the entire

*Note, though, that if one relaxes the condition of no normal flow through these boundaries, so that they are no longer true material surfaces, then this restriction on the flux through these boundaries is also relaxed, a point we will return to later.

eigensolution is growing on the fast time scale. We will show that it is indeed in this way that the adjustment to the Bondi-Gold theorem occurs in bounded fast dynamos.

We then also consider some of the implications of this adjustment for the different symmetries of the field and the flow. In particular, we will show first that, for a given flow **u**, fields of dipolar and quadrupolar type have very similar growth rates and indeed even eigensolutions. And then we consider the implications of this result in turn for the two flows **u** and $-\mathbf{u}$. We show that the eigensolutions are quite distinct, but the growth rates are still very similar.

2. THE CHOICES OF FLOW U

We consider an axisymmetric flow in a spherical shell lying between $r_i = 1/2$ and $r_o = 3/2$. The great advantage in taking a two-dimensional rather than a three-dimensional flow is that the field then also becomes effectively two-dimensional, in the sense that one may focus on individual azimuthal modes $\exp(im\phi)$ of the field in isolation. It is this feature that will enable us to increase R_m up to 10^5.

In trying to decide which such flows are most likely to act as fast dynamos, we turn once again to the frozen flux theorem, which suggests that a flow will be efficient at stretching field lines if it is efficient at stretching material lines. Finn and Ott (1988) have suggested, and Klapper and Young (1995) have proved, that in order to act as a fast dynamo, a smooth flow must be chaotic. If it is not, it will simply not stretch material lines, and hence magnetic field lines, efficiently enough to amplify the field on the fast time scale. Our flow must therefore be chaotic, which for a two-dimensional flow means it must be time-dependent, but this time-dependence is a price well worth paying.

As in I, we take this time-dependent flow to be of the form

$$\mathbf{u} = \nabla \times [r^{-1} f(r, t) \sin\theta \cos\theta \, \hat{\mathbf{e}}_\phi] + r\omega(r, t) \sin\theta \, \hat{\mathbf{e}}_\phi. \tag{2.1}$$

The angular structure is thus narrowly prescribed, which will turn out to be important, but the time-dependent radial structure is quite

arbitrary. For this radial structure, we take

$$f(r,t) = (r-1/2)(r-3/2)/2\sin[4\pi r + \delta\sin(\pi/4\,t)], \tag{2.2a}$$

$$\omega(r,t) = 2\sin[4\pi r + \delta\sin(\pi/4\,t)], \tag{2.2b}$$

again essentially as in I. The parabolic envelope $(r-1/2)(r-3/2)$ in f again enforces the no normal flow boundary condition at the inner and outer boundaries of the spherical shell, and the $\sin[4\pi r + \delta\sin(\pi/4\,t)]$ term again represents four circulation cells, as shown in Figure 1(a). The $\delta\sin(\pi/4\,t)$ time-dependence then shakes them back and forth in r with some amplitude δ. In I we considered only the case $\delta = 1$; here we consider $\delta = 0$, 1 and 2. The case $\delta = 0$ of course corresponds to a time-independent, and hence non-chaotic flow, and does indeed yield only a slow dynamo. Obtaining the $\delta = 0$ growth rates is nonetheless of interest, if only because the contrast with the $\delta = 1$ and 2 growth rates demonstrates all the more vividly that the latter do seem to yield fast dynamos. Also, in I we considered only the flow $\mathbf{u}$; here we consider both $\mathbf{u}$ and $-\mathbf{u}$. In plane periodic geometry $\mathbf{u}$ and $-\mathbf{u}$ are typically identical, merely shifted by half a period in space and/or time, but for the flows considered here they are distinct, which will turn out to have

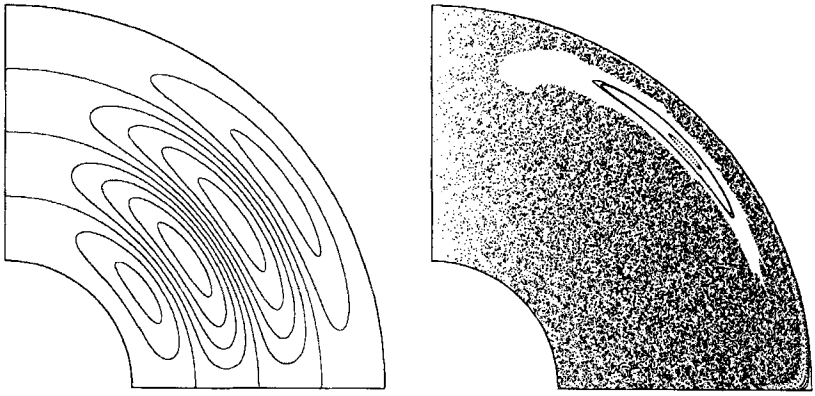

FIGURE 1(a) Instantaneous streamlines, at $t = 0$ modulo T, of the flow $\mathbf{u}_m = \nabla \times [r^{-1} f(r,t)\sin\theta\cos\theta\,\hat{\mathbf{e}}_\phi]$ in the meridional plane. (b) Poincaré section of the flow $\mathbf{u}_m$. Points are plotted at $t = 0$ modulo T.

interesting consequences, as noted above. [Incidentally, we have been asked by a referee to clarify what we mean by the flow $-\mathbf{u}$; do we mean $-\mathbf{u}(t)$ or $-\mathbf{u}(-t)$? In general the two are not the same, and indeed may have different chaotic properties, with $-\mathbf{u}(-t)$ necessarily having the same properties as $\mathbf{u}(t)$, but $-\mathbf{u}(t)$ possibly having different properties. However, for our particular time-dependence $-\mathbf{u}(t)$ and $-\mathbf{u}(-t)$ are the same, merely shifted by half a period in time, and so this distinction does not arise.]

In I we already verified that the $\delta = 1$ flow is chaotic. To verify that the $\delta = 2$ flow is also chaotic, we show in Figure 1(b) a Poincaré section of the particle paths in the meridional plane. This is obtained by numerically integrating forward in time the ordinary differential equations

$$\frac{dr}{dt} = u_r(r, \theta, t), \qquad r\frac{d\theta}{dt} = u_\theta(r, \theta, t), \tag{2.3}$$

where u_r and u_θ are given by this meridional circulation $\mathbf{u}_m = \nabla \times [r^{-1} f(r, t) \sin\theta\cos\theta\, \hat{\mathbf{e}}_\phi]$. If one then plots the positions of a few randomly selected test particles after successive periods $T = 8$ of the flow, one obtains Figure 1(b), demonstrating that this flow has a very large region of chaotic particle paths, and so should be a likely candidate for fast dynamo action. And again, for each δ the chaotic properties of $\mathbf{u}$ and $-\mathbf{u}$ are the same, so of our six distinct flows $\pm\mathbf{u}$, each with $\delta = 0$, 1 and 2, two are non-chaotic and four are chaotic.

Two other quantities of interest about these four chaotic flows are the largest Lyapunov exponent, which turns out to be about 0.15 for $\delta = 1$ and 0.14 for $\delta = 2$, and the topological entropy, which turns out to be about 0.31 for $\delta = 1$, and 0.36 for $\delta = 2$. The largest Lyapunov exponent is the average rate at which the flows stretch infinitesimal line elements; the topological entropy is the average rate at which they stretch finite line elements. Now, it turns out that the rate at which infinitesimal line elements are stretched does not necessarily bound the growth rate of the field, but the rate at which finite line elements are stretched does (Klapper and Young, 1995). And we will discover in the next section that the fast dynamo growth rates of these flows are greater than 0.15 but less than 0.3.

3. NUMERICAL SOLUTION FOR B

Having decided upon the imposed flows, and verified that they are chaotic for shaking amplitudes $\delta = 1$ and 2, we return to the induction equation (1.1), and present a numerical solution to it. Again as in I, we begin by using $\nabla \cdot \mathbf{B} = 0$ to decompose the field as

$$\mathbf{B} = \nabla \times (g\hat{\mathbf{r}}) + \nabla \times \nabla \times (h\hat{\mathbf{r}}). \tag{3.1}$$

We then expand g and h as

$$g = \sum_{n=1}^{N} g_n(r)\, \mathrm{P}_{n_2}^m(\cos\theta) \exp(im\phi), \tag{3.2a}$$

$$h = \sum_{n=1}^{N} h_n(r)\, \mathrm{P}_{n_1}^m(\cos\theta) \exp(im\phi), \tag{3.2b}$$

where we are imposing a particular symmetry by choosing n_1 and n_2 appropriately. For this particular equatorial symmetry (2.1) of the flow, the field decouples into distinct dipolar (having $n_1 = 2n + m - 1$ and $n_2 = 2n + m - 2$) and quadrupolar (having $n_1 = 2n + m - 2$ and $n_2 = 2n + m - 1$) modes. In I we considered only dipole modes; here we consider both dipole and quadrupole modes, and in the process demonstrate that the corresponding fast dynamo growth rates and eigensolutions are very similar. Finally, note once again that by taking the flow to be axisymmetric, we may focus on each individual azimuthal mode $\exp(im\phi)$ of the field in isolation. We will consider only the $m = 1$ modes in detail here; the higher modes also appear to be excited, but at considerably smaller growth rates.

To obtain the evolution equations for $g_n(r)$ and $h_n(r)$, we calculate the r-components of (1.1) and its curl. Using the defining equation (Abramowitz and Stegun, 1968) for the associated Legendre functions $\mathrm{P}_n^m(\cos\theta)$, as well as the recursion relations

$$\cos\theta \mathrm{P}_n^m(\cos\theta) = A_n \mathrm{P}_{n+1}^m(\cos\theta) + B_n \mathrm{P}_{n-1}^m(\cos\theta), \tag{3.3a}$$

$$\sin\theta \frac{d}{d\theta} \mathrm{P}_n^m(\cos\theta) = nA_n \mathrm{P}_{n+1}^m(\cos\theta) - (n+1)B_n \mathrm{P}_{n-1}^m(\cos\theta), \tag{3.3b}$$

where

$$A_n \equiv \frac{n-m+1}{2n+1}, \qquad B_n \equiv \frac{n+m}{2n+1}, \tag{3.4}$$

one obtains after a little algebra,

$$\begin{aligned}\frac{\partial}{\partial t} h_n =& R_m^{-1}[h_n'' - n_1(n_1+1)h_n/r^2] \\ & - im\omega h_n + if_1 H_n^1 g_n + if_1 H_n^2 g_{n+1} \\ & + f_3 H_n^3 h_{n-1} + f_3 H_n^4 h_{n+1} + f_3 H_n^5 h_n \\ & + f_1 H_n^6 h'_{n-1} + f_1 H_n^7 h'_{n+1} + f_1 H_n^8 h'_n,\end{aligned} \tag{3.5a}$$

$$\begin{aligned}\frac{\partial}{\partial t} g_n =& R_m^{-1}[g_n'' - n_2(n_2+1)g_n/r^2] \\ & - im\omega g_n + \omega' G_n^1 h_{n-1} + \omega' G_n^2 h_n \\ & + if_4 G_n^3 h_{n-1} + if_4 G_n^4 h_n + if_3 G_n^5 h'_{n-1} + if_3 G_n^6 h'_n \\ & + if_2 G_n^7 h'_{n-1} + if_2 G_n^8 h'_n + if_1 G_n^7 h''_{n-1} + if_1 G_n^8 h''_n \\ & + f_3 G_n^9 g_{n-1} + f_3 G_n^{10} g_{n+1} + f_3 G_n^{11} g_n \\ & + f_2 G_n^{12} g_{n-1} + f_2 G_n^{13} g_{n+1} + f_2 G_n^{14} g_n \\ & + f_1 G_n^{12} g'_{n-1} + f_1 G_n^{13} g'_{n+1} + f_1 G_n^{14} g'_n,\end{aligned} \tag{3.5b}$$

for the dipole modes, and similarly for the quadrupole modes.

Note first that the entire angular structure has been subsumed into these coupling coefficients H_n^1 through H_n^8 and G_n^1 through G_n^{14}, given in terms of the A_n and B_n. In particular, note that according to (3.5a) h_n couples only to itself, $h_{n\pm1}$, g_n and g_{n+1}, and according to (3.5b) g_n couples only to itself, $g_{n\pm1}$, h_{n-1} and h_n. (Not surprisingly, in the corresponding quadrupole equations, h_n couples only to itself, $h_{n\pm1}$, g_{n-1} and g_n, and g_n couples only to itself, $g_{n\pm1}$, h_n and h_{n+1}.) It is because of the particularly simple angular structure (2.1) of the flow that the angular modes of the field couple only to adjacent modes.

Of course, these equations still contain the full radial structure of $g_n(r)$ and $h_n(r)$, as well as the time-dependent radial structure (2.2) of

the flow. Note, in particular, the occurrence of ω, ω', and

$$f_1 \equiv f/r^2, \qquad f_2 \equiv f_1', \tag{3.6a}$$

$$f_3 \equiv f'/r^2, \qquad f_4 \equiv f_3', \tag{3.6b}$$

throughout (3.5). The radial structure of g_n and h_n is implemented by finite-differencing. This has the very considerable advantage that the radial grid points then also couple only to adjacent grid points.

These evolution equations (3.5), together with the insulating boundary conditions

$$g_n = 0, \quad h_n' - \frac{n_1 + 1}{r_i} h_n = 0, \quad \text{at} \quad r = r_i, \tag{3.7a}$$

$$g_n = 0, \quad h_n' + \frac{n_1}{r_o} h_n = 0, \qquad \text{at} \quad r = r_o, \tag{3.7b}$$

constitute the system we wish to solve. The equations were time-stepped forward using a second-order Runge-Kutta method, modified to treat the diffusive terms implicitly. Because the angular modes and radial grid points couple only to adjacent modes and grid points, one can run the code reasonably efficiently even at very large truncations. Although these equations will always settle down to a well-defined eigensolution at any finite R_m, one must expect that these eigensolutions will exhibit increasingly fine structure with increasingly large R_m. Moffatt and Proctor (1985) have demonstrated that they will exhibit structure as fine as $O(R_m^{-1/2})$. As the magnetic Reynolds number tends to infinity, these eigenfunctions thus tend toward generalized, presumably fractal functions (Du and Ott, 1993). It is the need to resolve this increasingly fine structure that makes the calculations so difficult, but also so interesting. The largest truncation used in this work is $N = 768$ angular modes times $M = 1500$ radial grid points, and is sufficient to resolve this structure for R_m up to 10^5. The code was run on the parallel processor Cray T3D, as described by Hollerbach (1995).

4. RESULTS

According to Floquet theory, the eigensolutions of (3.5) should be of the form

$$\mathbf{B} = \exp[(\Lambda_r + i\Lambda_i)t]\,\mathbf{b}(t), \tag{4.1}$$

where $\Lambda \equiv \Lambda_r + i\Lambda_i$ is the Floquet exponent, and $\mathbf{b}(t)$ has the same periodicity $T=8$ as the flow $\mathbf{u}(t)$. Then Λ_r is the average growth rate over a period; it is this quantity that must tend to some nonzero value as the magnetic Reynolds number tends to infinity if the flow is to be a fast dynamo. Then Λ_i is just the average phase drift over a period; the two terms $\exp(i\Lambda_i t)$ and $\exp(im\phi)$ combine to give a shift in longitude over each period. This phase shift is not particularly interesting, though, and can easily be removed before the solutions are examined.

We found that the eigensolutions are indeed of the form (4.1). Starting the code with random initial conditions for the g_n and h_n, we found that the dominant eigensolutions established themselves after one or two dozen periods, with this time being largely independent of R_m, incidentally, at least for the $\delta=1$ and 2 cases. Figure 2 shows the dipolar and quadrupolar growth rates Λ_r as functions of R_m, and for the $\delta=1$ and 2 cases they do appear to level off, to about 0.21 for all four $\delta=1$ cases, and 0.26–0.27 for all four $\delta=2$ cases. One notes that the entire dipolar and quadrupolar growth rate curves are remarkably similar for both the $\delta=1$ and 2 cases; we will see in a moment why this is so. In both cases the growth rates in the limit of large R_m are thus greater than the largest Lyapunov exponent, as they may be, but less than the topological entropy, as they must be (Klapper and Young, 1995). The growth rates seem to level off sooner for $\delta=2$ than for $\delta=1$, and at a greater value. It is not clear why they level off sooner, but presumably they level off at a greater value because the topological entropy is greater, 0.36 versus 0.31.

In striking contrast to the $\delta=1$ and 2 cases, the growth rates for the four $\delta=0$ cases do not level off with increasing R_m. Instead, they tend to zero, apparently as $O(R_m^{-1/2})$. Not surprisingly, the time scale on which these eigensolutions establish themselves then also increases with R_m. Ironically, it is thus actually easier to obtain the $\delta=1$ and 2 fast modes than the $\delta=0$ slow modes (which is why we computed only a few isolated points on these $\delta=0$ growth rate curves).

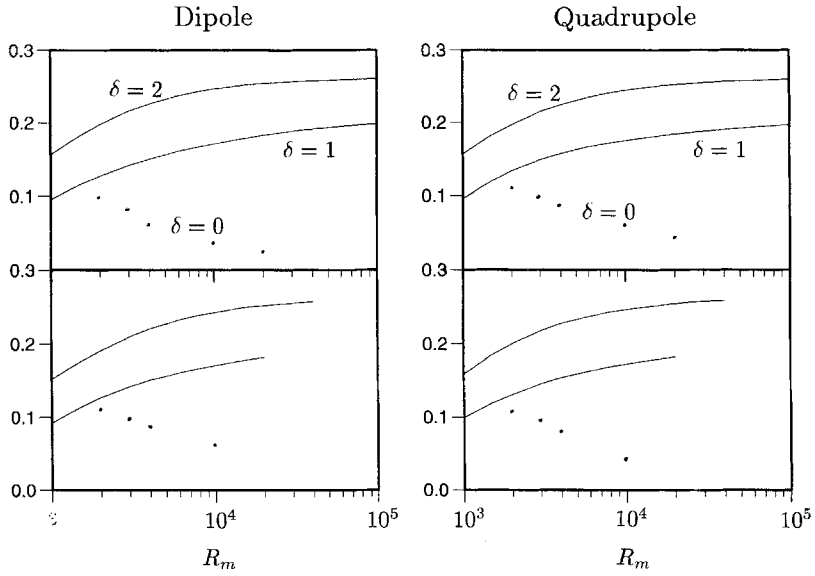

FIGURE 2 The growth rates Λ_r of the dipolar and quadrupolar $m=1$ modes, plotted against R_m on a logarithmic scale. In both cases the top panel is for $+\mathbf{u}$, the bottom panel for $-\mathbf{u}$. The growth rate curves for $-\mathbf{u}$ are not extended as far as for $+\mathbf{u}$ merely because the calculations are very expensive at large R_m, and the similarities are already apparent.

Figure 3 shows the periodic structure of the dipolar $+\mathbf{u}$, $\delta=2$ eigensolutions $\mathbf{b}(t)$ at $t=0, 2, 4, 6$ modulo 8 for $R_m=4000$, 16000, and 64000. This phase drift has been removed by focusing on the particular meridional plane for which $\int b_\phi \, dS = 0$. The field consists of a strong flux rope b_r on the z-axis, from which flux sheets b_θ are then drawn out at the instantaneous positions of the stagnation points. (Figure 4 shows these flux ropes in more detail, by showing cross-sections through them.) These solutions are very similar to the (also dipolar) $\delta=1$ eigensolutions presented in I; the main difference being that the instantaneous positions of the stagnation points move by twice as much for $\delta=2$ as for $\delta=1$. In both cases the field generation appears to arise due to heteroclinic tangling between these moving stagnation points.

Note also that, as expected, the field exhibits structure on a very fine scale, consistent with an $O(R_m^{-1/2})$ scaling. Not only do these structures

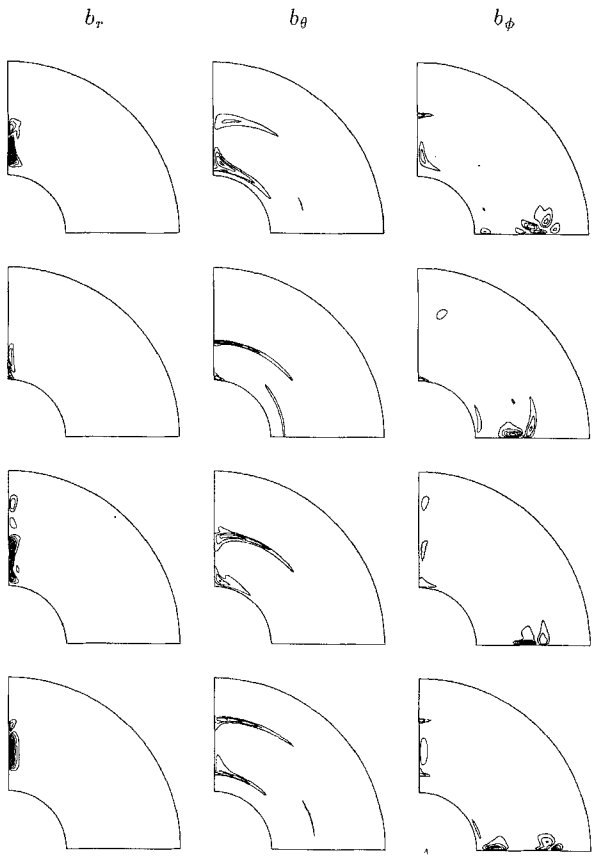

FIGURE 3a The structure of the $+\mathbf{u}$ dipolar field $\mathbf{b}(t)$ at $R_m = 4000$, in the particular meridional plane for which $\int b_\phi dS = 0$. From top to bottom $t = 0, 2, 4, 6$ mod 8; from left to right contours of b_r, b_θ, b_ϕ. Contour intervals of one throughout, with the zero contours suppressed to focus on the dominant structures. The field has been normalized such that the magnetic energy $\frac{1}{2}\int |\mathbf{b}|^2 dV = 1$.

become finer as R_m becomes larger, they appear to break up into multiple strands. This is exactly what one would expect if the eigensolutions are tending toward generalized fractal functions. As R_m becomes larger and larger one sees more and more "iterations" of this heteroclinic tangling before one finally reaches the $O(R_m^{-1/2})$ diffusion scale.

Turning now to the central issue, the adjustment to the Bondi-Gold theorem, Tables I and II show, respectively, the inner and outer pole

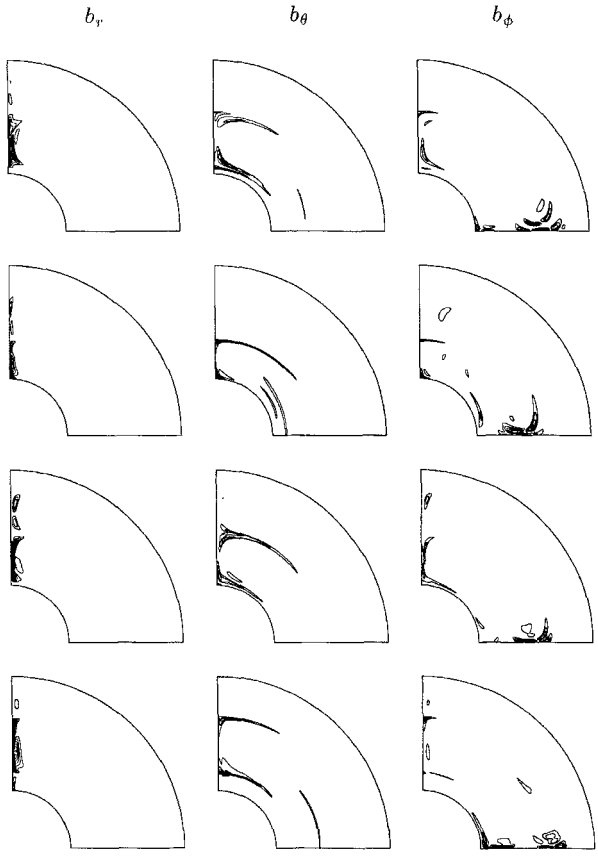

FIGURE 3b As in Figure 3(a), but at $R_m = 16000$.

strengths at $t = 0, 2, 4, 6$, for these three values of R_m. The field has been normalized such that the magnetic energy $\frac{1}{2}\int |\mathbf{b}|^2 \, dV = 1$ at $t = 0$. One notes a clear tendency for these pole strengths to decrease with increasing R_m. The outer pole strengths decrease very rapidly, by a factor of around ten for each four-fold increase in R_m. The inner pole strengths decrease more slowly, and at a more variable rate. That they decrease more slowly is presumably due simply to the fact that these eigensolutions happen to push against the inner boundary more than against the outer boundary. That they decrease at a more variable rate is then presumably due to the fact that as a result of this pushing

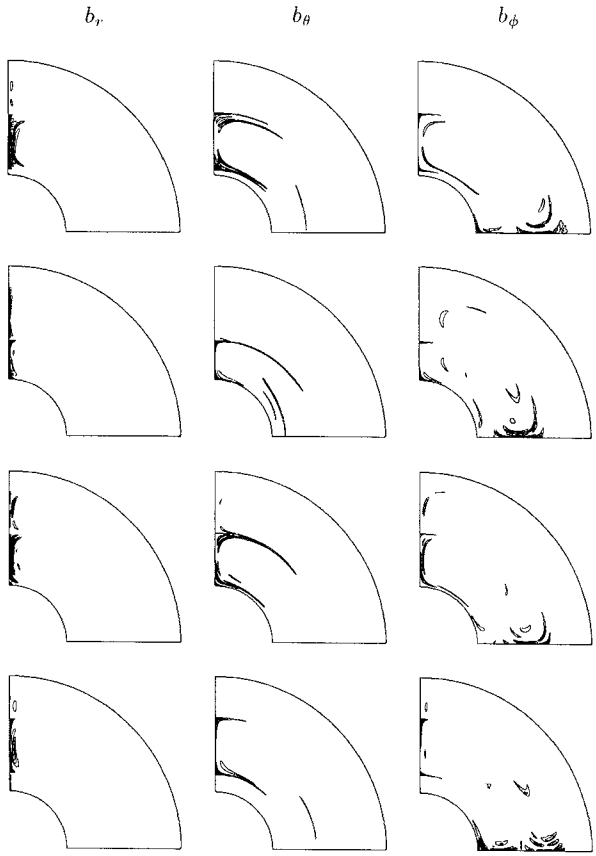

FIGURE 3c As in Figure 3(a), but at $R_m = 64000$.

against the boundary, the inner boundary effectively sees more of the fractal nature of the field than does the outer boundary. However, one notes that even at $t=2$, when the field is pushed against the inner boundary most strongly, and consequently the inner pole strength is largest, it still decreases with increasing R_m. That is, for larger and larger R_m, the inner boundary sees less and less of the field even when it is pushed against that boundary most strongly. That would suggest that as R_m tends to infinity, the pole strengths tend to zero even when the field pushes against the boundary the most.

Figure 5 shows the periodic structure of the quadrupolar $+\mathbf{u}$, $\delta=2$ eigensolution for $R_m=$ 16000, and one notes that it is remarkably

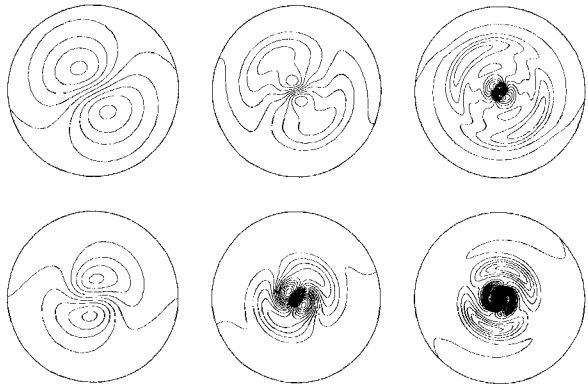

FIGURE 4 Cross-sections through these flux ropes on the z-axis. The top row corresponds to $t=0$ mod 8, the bottom row to $t=4$ mod 8. From left to right $R_m=$ 4000, 16000, and 64000. All sections are at $r=0.75$, cover the innermost five degrees in θ, and show contours of b_r, with contour intervals of five. One notes clearly the increasingly fine structure with increasing R_m; one also notes how these structures break up into multiple strands. (Incidentally, these cross-sections also illustrate nicely the underlying $m=1$ azimuthal dependence of all of these solutions.)

similar to the corresponding dipolar solution in Figure 3(b). We believe this to be the reason why the dipolar and quadrupolar growth rate curves are so similar: Because both eigensolutions are concentrated on the z-axis, away from the equator, they are largely unaffected by the different symmetries there. One can show in fact that for large R_m the eigensolutions must become less and less affected by the different equatorial symmetries, by noting that for our choice of meridional circulation the equator is itself a streamsurface, so the two hemispheres are only coupled by diffusion, and so they must become increasingly decoupled for increasingly large R_m.

TABLE I The inner pole strengths $\int_{r=r_i} |b_r|\, dS$ of the dipolar $+\mathbf{u}$, $\delta=2$ eigensolutions, at $t=$ 0, 2, 4, 6 mod 8, for the three values of R_m, with the field normalized by $\frac{1}{2}\int |\mathbf{b}(0)|^2\, dV = 1$

R_m	$t=0$	$t=2$	$t=4$	$t=6$
4000	3.00×10^{-2}	8.40×10^{-2}	5.44×10^{-2}	2.09×10^{-2}
16000	1.95×10^{-2}	7.79×10^{-2}	3.30×10^{-2}	1.08×10^{-2}
64000	0.79×10^{-2}	6.34×10^{-2}	2.42×10^{-2}	1.01×10^{-2}

TABLE II The outer pole strengths $\int_{r=r_o} |b_r| \, dS$ of the dipolar $+\mathbf{u}$, $\delta = 2$ eigensolutions, at $t = 0, 2, 4, 6$ mod 8, for the three values of R_m, with the field normalized by $\frac{1}{2}\int |\mathbf{b}(0)|^2 \, dV = 1$

R_m	$t=0$	$t=2$	$t=4$	$t=6$
4000	15.85×10^{-4}	13.05×10^{-4}	7.05×10^{-4}	6.08×10^{-4}
16000	1.18×10^{-4}	1.24×10^{-4}	0.76×10^{-4}	0.60×10^{-4}
64000	0.08×10^{-4}	0.11×10^{-4}	0.07×10^{-4}	0.05×10^{-4}

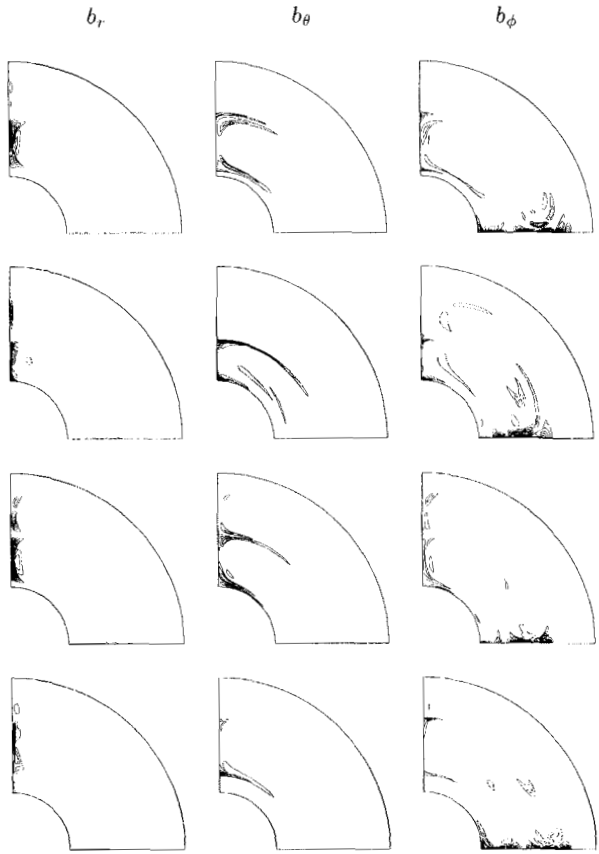

FIGURE 5 The structure of the $+\mathbf{u}$ quadrupolar field $\mathbf{b}(t)$ at $R_m = 16000$, in the particular meridional plane for which $\int b_\phi dS = 0$. From top to bottom $t = 0, 2, 4, 6$ mod 8; from left to right contours of b_r, b_θ, b_ϕ. Contour intervals of half throughout.

This would suggest, incidentally, that if the equator were not a streamsurface one might obtain very different results, and indeed one would: if the symmetry of the circulation were such that the equator were not a streamsurface one would not obtain a decoupling into distinct dipole and quadrupole modes at all. For the equator to be a streamsurface is thus a necessary condition for d/q decoupling. Interestingly enough, however, it is not a sufficient condition; unless the symmetry of the angular velocity is also as in (2.1), one will not obtain this d/q decoupling even if the symmetry of the meridional circulation is as in (2.1). One could thus have a solution where the two hemispheres are almost completely decoupled according to the argument given above, but the solutions are nevertheless not decoupled into distinct dipole and quadrupole modes. It is not immediately clear what one would obtain in this case.

However, returning to the eigensolutions that we have obtained, we note that because both eigensolutions are also concentrated away from the boundaries (that after all is the main conclusion of this work), they are also largely unaffected by the slightly different external potential matches there. In other words, we are seeing essentially the same eigensolution twice; the fact that both their growth rates and structures are essentially the same just demonstrates once again how unimportant the boundaries (and the equatorial symmetry) are for these solutions.

We believe it is this feature that also explains why the $\mathbf{u}$ and $-\mathbf{u}$ growth rate curves are so similar. Proctor (1977) has shown that for a certain "comparison problem" in which one imposes not the boundary conditions (3.7), but simply $g_n = h_n = 0$, the dipolar/quadrupolar growth rates for $\mathbf{u}$ should be exactly the same as the quadrupolar/dipolar growth rates for $-\mathbf{u}$. Well, once again the main conclusion of this work is that the eigensolutions are concentrated away from the boundaries, that is, they are essentially adjusting themselves to Proctor's modified boundary conditions. One might therefore expect the d/q growth rates for $-\mathbf{u}$ to be similar to the q/d growth rates for $\mathbf{u}$, and since we just showed that the two growth rates for $\mathbf{u}$ are themselves similar, one might in fact expect all four growth rate curves for $\pm\mathbf{u}$ to be similar. (Strictly speaking, Proctor only proved his result for steady flows, and so it is not directly applicable here. However, the excellent agreement we obtain suggests it is in fact valid even for unsteady flows.)

Interestingly enough, however, the eigensolutions for $\pm\mathbf{u}$ are not quite so similar. Figures 6 and 7 show, respectively, the dipolar and quadrupolar $-\mathbf{u}$, $\delta = 2$ eigensolutions for $R_m = 16000$, and one notes first that these two $-\mathbf{u}$ eigensolutions are also very similar, just as the two $+\mathbf{u}$ eigensolutions were. The $-\mathbf{u}$ eigensolutions again consist of a strong flux rope b_r on the z-axis, from which flux sheets b_θ are again drawn out at the instantaneous positions of the stagnation points. However, because the flow is now reversed, the roles of all the

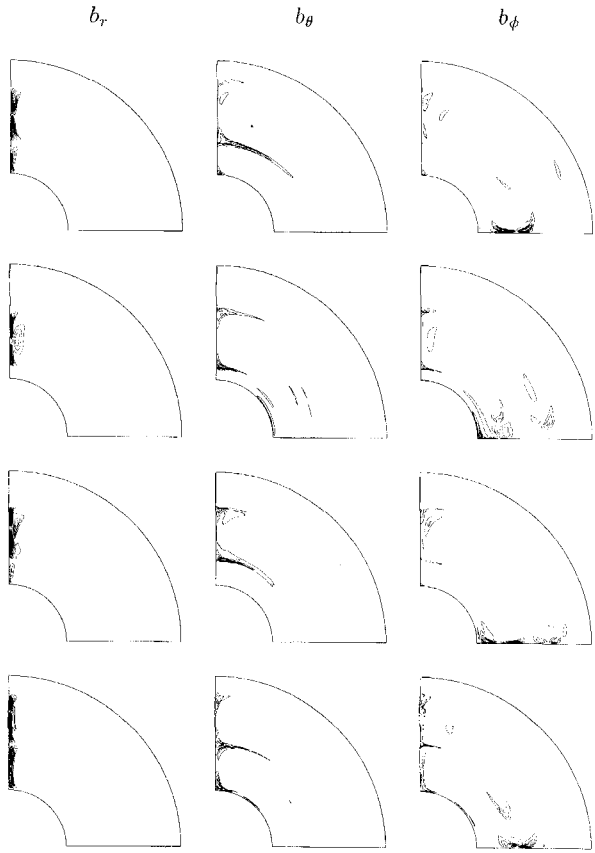

FIGURE 6 The structure of the $-\mathbf{u}$ dipolar field $\mathbf{b}(t)$ at $R_m = 16000$, in the particular meridional plane for which $\int b_\phi dS = 0$. From top to bottom $t = 0, 2, 4, 6 \bmod 8$; from left to right contours of b_r, b_θ, b_ϕ. Contour intervals of one throughout.

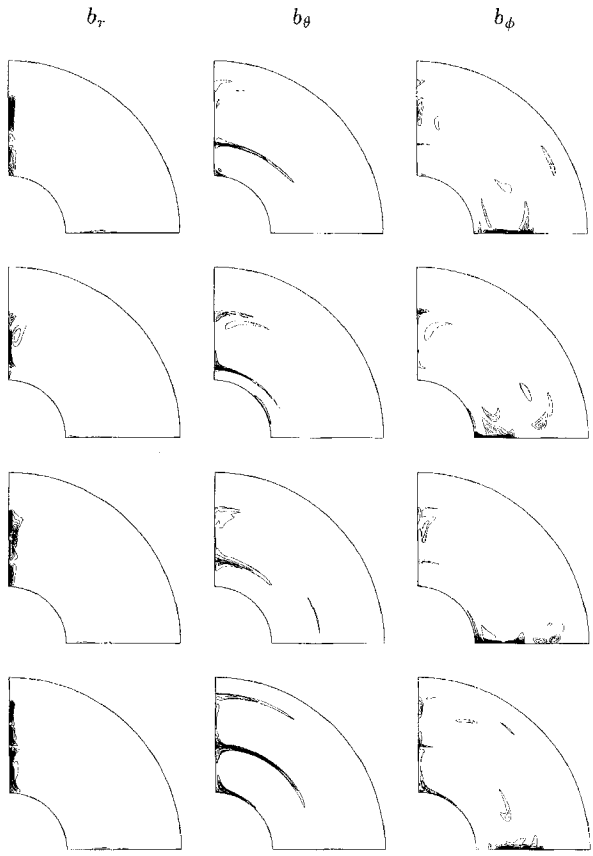

FIGURE 7 The structure of the $-\mathbf{u}$ quadrupolar field $\mathbf{b}(t)$ at $R_m = 16000$, in the particular meridional plane for which $\int b_\phi dS = 0$. From top to bottom $t = 0, 2, 4, 6 \bmod 8$; from left to right contours of b_r, b_θ, b_ϕ. Contour intervals of half throughout.

stagnation points are also reversed. That is, the stagnation points where the field is now being drawn out from the axis are the ones where previously the field was being swept in to the axis, and vice versa. We thus see that although the eigensolutions for $\pm\mathbf{u}$ are broadly similar in their overall structure, the details are quite distinct, because the flows are distinct. Despite this, their growth rates are very similar, as noted above. [See also Bayly and Childress (1989) for a problem where the direct and adjoint eigensolutions are completely different,

with one being fractal and the other smooth, but where the growth rates are nonetheless very similar.]

5. CONCLUSION

In this work we have considered the adjustment to the Bondi-Gold theorem in the limit $R_m \to \infty$. Because it is a singular limiting process, one must be very careful in applying to the limit $R_m \to \infty$ results, such as the Bondi-Gold theorem, that have only rigorously been proven in the limit $R_m \equiv \infty$. Formally, the Bondi-Gold theorem states that in the limit $R_m \equiv \infty$ the external field cannot be amplified. We have demonstrated that in this particular case there is a link between these two limits $R_m \equiv \infty$ and $R_m \to \infty$, which comes about in the following way: At any finite R_m, the entire field, including the external field, is amplified on the fast time scale. As R_m then increases, this external field decreases, relative to the internal field. That is, as R_m becomes greater and greater, there is simply less and less external field to be amplified, until at infinite R_m there is no external field, and one is left simply with Rädler's "invisible dynamo."

We then also considered some of the implications of this adjustment for the different symmetries of the field and the flow. We noted that this adjustment to the Bondi-Gold theorem turns out to be precisely what is required for Proctor's (1977) "comparison problem" to apply (again assuming it is valid for unsteady flows as well), which then presumably explained why the growth rate curves were so similar for the four possible states consisting of dipolar/quadrupolar fields and $\pm\mathbf{u}$ flows. Despite these similarities in the growth rates, however, the eigensolutions for $\pm\mathbf{u}$ were not so similar; both sets of eigensolutions consisted of flux ropes on the z-axis, but the positions from which flux sheets were then drawn out from the axis were different for the two flows. We thus ended up with four distinct modes all having very similar growth rates, but one of two different spatial structures.

Finally, we return briefly to the original astrophysical motivation for this work, and consider the implications for a body such as the Sun. While the Sun today is not in the linear, kinematic regime where the magnetic field grows exponentially without limit, the Bondi-Gold theorem in fact applies in the dynamic regime as well, and suggests

that the Sun's pole strength should be roughly constant throughout the solar cycle, as has indeed been suggested on the basis of actual observations (Golub *et al.*, 1979). Still, to say that the pole strength should be roughly constant throughout the cycle begs the question how it got to be as large as it is in the first place – the results presented here suggest it ought to be vanishingly small, at least in comparison with the internal field. Unless one is willing to postulate an impossibly large internal field, one needs some mechanism which will enhance the external field relative to the internal field. One possible effect is the escape of magnetised material through the surface into the atmosphere. That this happens is clearly shown in the videos obtained via the Yohkoh soft X-ray satellite (Svestka *et al.*, 1995). The rise of this material is initiated by magnetic buoyancy in the Sun's interior (Parker, 1984); it then emerges into the Sun's atmosphere, violating the condition of no normal flow assumed in the derivation of the Bondi-Gold theorem. Subsequently nearly all this material drains back along the field lines towards the surface, but a small fraction, together with its associated magnetic flux, is lost into the solar wind. Parker's paper discusses the complexities of this process in some detail; the results presented here suggest that its proper inclusion may be crucial for understanding why stellar magnetic fields are actually observable from the outside, rather than being confined entirely to the inside, as would otherwise be the case.

Acknowledgements

We thank Isaac Klapper for valuable discussions on the relationship between the largest Lyapunov exponent, the topological entropy, and the fast dynamo growth rate. We thank Graeme Sarson for suggesting the use of the flow $-\mathbf{u}$. The calculations described here were done in part on the Cray T3D at the Advanced Computing Laboratory of Los Alamos National Laboratory, Los Alamos, NM 87545, USA.

References

Abramowitz, M. and Stegun, I. A. (eds), *Handbook of mathematical functions*. New York: Dover (1968).

Bayly, B.J. and Childress, S., "Unsteady dynamo effects at large magnetic Reynolds numbers," *Geophys. Astrophys. Fluid Dynam.* **49**, 23–43 (1989).

Bondi, H. and Gold, T., "On the generation of magnetism by fluid motion," *Mon. Not. R. Astr. Soc.* **110**, 607–611, (1950).
Childress, S. and Gilbert, A. D., *Stretch, Twist, Fold: The Fast Dynamo*. New York: Springer (1995).
Du, Y.S. and Ott, E., "Fractal dimensions of fast dynamo magnetic fields," *Physica* D **67**, 387–417 (1993).
Dudley, M. L. and James, R. W., "Time-dependent kinematic dynamos with stationary flows," *Proc. R. Soc. Lond.* A **425**, 407–429 (1989).
Finn, J. M. and Ott, E., "Chaotic flows and fast magnetic dynamos," *Phys. Fluids* **31**, 2992–3011 (1988).
Galloway, D. J. and Frisch, U., "Dynamo action in a family of flows with chaotic streamlines," *Geophys. Astrophys. Fluid Dynam.* **36**, 53–83 (1986).
Galloway, D. J. and Proctor, M. R. E., "Numerical calculations of fast dynamos in smooth velocity fields with realistic diffusion," *Nature* **356**, 691–693 (1992).
Golub, L., Davis, J. M. and Krieger, A. S., "Anticorrelation of X-ray bright points with sunspot number, 1970-1978," *Astrophys. J. Lett.* **229** 145–150 (1979).
Hollerbach, R., "Fast dynamo action in spherical geometry: Numerical calculations using parallel virtual machines," *Comput. Phys.* **9**, 460–463 (1995).
Hollerbach, R., Galloway, D. J. and Proctor, M. R. E., "Numerical evidence of fast dynamo action in a spherical shell," *Phys. Rev. Lett.* **74**, 3145–3148 (1995).
Klapper, I. and Young, L. S., "Rigorous bounds on the fast dynamo growth rate involving topological entropy," *Comm. Math. Phys.* **173**, 623–646 (1995).
Moffatt, H. K., *Magnetic Field Generation in Electrically Conducting Fluids*. Cambridge: Cambridge University Press (1978).
Moffatt, H. K., "A self-consistent treatment of simple dynamo systems," *Geophys. Astrophys. Fluid Dynam.* **14**, 147–166 (1979).
Moffatt, H. K. and Proctor, M. R. E., "Topological constraints associated with fast dynamo action," *J. Fluid Mech.* **154**, 493–507 (1985).
Otani, N. F., "A fast kinematic dynamo in two-dimensional time-dependent flows," *J. Fluid Mech.* **253**, 327–340 (1993).
Parker, E. N., *Cosmical Magnetic Fields: their Origin and their Activity*. Oxford: Clarendon (1979).
Parker, E. N., "Magnetic buoyancy and the escape of magnetic fields from stars," *Astrophys. J.* **281**, 839–845 (1984).
Ponty, Y., Pouquet, A. and Sulem , P. L., "Dynamos in weakly chaotic two-dimensional flows," *Geophys. Astrophys. Fluid Dynam.* **79**, 239–257 (1995).
Proctor, M. R. E., "The role of mean circulation in parity selection by planetary magnetic fields," *Geophys. Astrophys. Fluid Dynam.* **8**, 311–324 (1977).
Rädler, K.-H., "On dynamo action in the high-conductivity limit," *Geophys. Astrophys. Fluid Dynam.* **20**, 191–211 (1982).
Svestka, Z., Farnik, F. , Hudson, H. S. , Uchida, Y., Hick, P. and Lemen, J. R., "Large-scale active coronal phenomena in Yohkoh SXT images. 1. Post-flare giant arches rising with constant speed," *Solar Phys.* **161**, 331–363 (1995).
Vainshtein, S.I. and Zeldovich, Ya. B., "Origin of magnetic fields in astrophysics," *Sov. Phys. Usp.* **15**, 159–172 (1972).
Zheligovsky, V. A., "A kinematic magnetic dynamo sustained by a Beltrami flow in a sphere," *Geophys. Astrophys. Fluid Dynam.* **73**, 217–254 (1993).